



Dual-phase hetero-structured strategy to improve ductility of a low carbon martensitic steel

J.X. Huang^a, Y. Liu^a, T. Xu^a, X.F. Chen^{a,b}, Q.Q. Lai^c, L.R. Xiao^a, Z.Y. Pan^a, B. Gao^{a,**}, H. Zhou^{a,*}, Y.T. Zhu^{a,d}

^a Nano and Heterogeneous Materials Center, School of Materials Science and Engineering, Nanjing University of Science and Technology, Nanjing, 210094, China

^b School of Engineering Science, University of Chinese Academy of Sciences, Beijing, 100049, China

^c Herbert Gleiter Institute of Nanoscience, Nanjing University of Science and Technology, Nanjing, 210094, China

^d Department of Materials Science and Engineering, City University of Hong Kong, 999077, Hong Kong, China

ARTICLE INFO

Keywords:

Heterostructured materials
Hetero-deformation induced stress
Low-carbon martensitic steel
Nano-lamellae
Dual-phase structure

ABSTRACT

Martensitic transformation significantly increases the strength of low-carbon steels, while it is usually at expense of the formability and ductility. In order to further improve the mechanical properties of low carbon martensitic steel, the strategy of dual-phase heterostructure was proposed. The steel with nano-lamellar structure in size of 83 nm was produced by cyclic annealing & cold rolling (AnnCR) on the martensitic structure. Then, the ultrafine-grained heterostructured dual-phase (UFG-HSDP) steels with outstanding combination of strength and ductility were achieved by subsequent short-time intercritical annealing. A promising heterostructure of soft ferrite grains completely embedded in hard martensite grains was formed in the sample annealed at 820 °C. A high strength of ~1.1 GPa, close to the as-quenched full martensite steel, was retained in the HSDP steel. While, the uniform elongation was significantly improved to 6% by tailoring the dual-phase distribution. Hetero-deformation induced (HDI) stress, derived from the mechanical incompatibility of the dual-phase, is proposed to provide an extra strain hardening in the HSDP steels. Detailed microstructure analysis indicates that geometrically necessary dislocations piled-up near the zone interfaces produce a long-range back stress in the ferrite zones as well as a corresponding forward stress in the martensite zones, collectively resulting in the hetero-deformation induced (HDI) stress.

1. Introduction

Among the steel communities, low-carbon low-alloy steel is widely applied in building and transport for its low cost and good formability. However, the low strength usually limits its further industrial applications. Utilizing martensitic transformation and refining grains to ultra-fine/nano scale are widely used methods to improve the strength of low carbon steels. The as-quenched martensite exhibits high-strength due to its distinct fine microstructure and high density of defects. The as-quenched martensite phase, however, shows extremely low ductility and poor formability [1]. In addition, the ultrafine-grained/nanocrystalline (UFG/NS) materials usually show extraordinarily high strength at the expense of ductility, owing to the limited strain hardening capacity [2,3]. It has been reported that appropriate post-heat treatment can improve the ductility of the

martensite and UFG/NS materials, however, the strength is decreased due to the dissolved martensitic structure, recovery of dislocations or recrystallization [4,5]. In order to obtain the steels with high performance, many advanced thermo-mechanical processing routes [6–9] and novel heat treatment approaches [10,11] have been developed. Moreover, the recent third-generation advanced high-strength steels utilize the quenching & partitioning processing to produce the Q&P steels mainly containing martensite, ferrite and retained austenite [12–14], which produce a superior combination of strength and ductility. These advanced processing routes provide numerous inspirations for producing high-performance steels by tailoring the microstructural features, e. g., grain size and constituent phases.

In recent years, hetero-structured materials (HSMs) have attracted extensive attention for their impressive mechanical/functional properties [15–18]. HSMs are usually defined as materials that contain

* Corresponding author.

** Corresponding author.

E-mail addresses: gaobo@njust.edu.cn (B. Gao), hzhou511@njust.edu.cn (H. Zhou).

heterogeneous zones that have dramatic constitutive properties in the case of structural metallic materials [19,20]. It is found that the excellent mechanical properties are mainly due to the interaction between the hetero-zones. During deformation, notable strain partitioning is induced by mechanical incompatibility, leading to a strain gradient near zone boundaries [21,22]. Additional high density geometrically necessary dislocations (GNDs) form and pile-up near the zone interface, which produce the long-range back stress and forward stress in the soft and hard zones, collectively resulting in the hetero-deformation induced (HDI) stress [23,24]. Consequently, heterostructured materials usually exhibit higher strain hardening rate than uniform structural materials. The ideal microstructure in HSMs, which can introduce maximum hetero-deformation induced (HDI) stress, is proposed as a small amount of soft zone strictly constrained by the surrounding hard zone [20]. So far, many different HSMs have been developed, including gradient nanostructure [25,26], laminated structure [27,28], heterogeneous lamellar structure [15,29], harmonic structure [30], bimodal/multi-modal grains [31], etc.

In terms of low-carbon low-alloy steels, the high strength of martensite phase makes it analogous to the hard zones in HSMs, while the ferrite shows low strength and good ductility, which is the typical soft zones. Thus, the dual-phase structured steel is a natural hetero-structured model [19,20]. In addition, the proportions, morphologies and sizes of constituent phases can be tailored by flexibly manipulating the alloying compositions and thermomechanical processing routes [32, 33]. Hence, it is expected to obtain hetero-structured dual-phase (HSDP) steels by tuning microstructural heterogeneity, resulting in the soft ferrite surrounded by the martensite. In this regard, the formation of DP structure during intercritical annealing for low carbon steels involves a number of metallurgical phenomena, such as phase transformation, ferrite recrystallization and carbon diffusion, which are significantly affected by the initial microstructure prior to heat treatment [34]. It is suggested that the DP steels prepared from the severe deformed structure, i.e., rolled ferrite-martensite or rolled martensite, usually show excellent combination of strength and ductility, which is resulted from the fine initial structure [35–37]. The deformed materials with finer structure and higher density of defects promote phase transformation and recrystallization, leading to the ultrafine-grained DP structure with outstanding mechanical properties [38,39].

Thus, it is a promising way to produce ultra-fine heterostructure in DP steels, started by a nanocrystalline microstructure before intercritical annealing. However, the formability of martensitic structure is very poor, which is difficult to be deformed by conventional cold rolling [40]. Here, we proposed a novel cyclic annealing & cold-rolling (AnnCR) processing to extremely refine the microstructure of martensitic steel to nano-lamellae first. Then, the ultrafine-grain heterostructured dual-phase (UFG-HSDP) steel was obtained by subsequent intercritical annealing with short duration in order to further improve the mechanical properties of low-carbon martensitic steel. The microstructural evolution and mechanical properties of UFG-HSDP steels have been systematically studied. In addition, according to the cyclic load-unload-reload (LUR) tensile tests, the in-depth mechanisms of strengthening and ductilization of UFG-HSDP steels were discussed.

2. Experimental materials and methods

2.1. Experimental materials

The low-carbon steel (Fe-0.09C-0.24Si-1.96Mn, in wt.%) was used as the starting material. The critical temperature A_1 and A_3 were calculated using Equations (1) and (2), respectively [36]:

$$A_1 = 723 - 10.7Mn - 16.9Ni + 29.1Si + 16.9Cr + 290As + 6.38W \quad (1)$$

$$A_3 = 910 - 203C_{0.5} - 15.2Ni + 44.7Si + 31.5Mo + 104V + 13.1W \quad (2)$$

The temperatures of A_1 and A_3 were estimated as 709 °C and 860 °C,

respectively. The processing route to producing UFG-HSDP steels is shown in Fig. 1a. First, the steel sheet with a thickness of 5.5 mm was austenitized at 950 °C for 60 min, and then water quenched to obtain martensitic microstructure. Second, the steel sheet was deformed by the AnnCR processing, i.e., the sheets were rolled at room temperature to a thickness reduction of 10%, followed by annealing at 300 °C for 10 min and air cooling to room temperature. The cold rolling and annealing were repeated until the total thickness reduction reached up to 80%. Third, the intercritical annealing was performed at 780 °C, 800 °C and 820 °C for 1 min, followed by water quenching. Before annealing, the furnace was preheated to the designated temperatures and hold about 30 min.

2.2. Tests of mechanical properties

Microhardness was measured by using a HMV-G hardness tester under a load of 200 g and with a holding time of 15 s. Average microhardness was acquired by averaging at least ten indentations for each sample. The dog bone-shaped tensile specimens with a gauge length of 10 mm and width of 2.5 mm, as shown in Fig. 1b, were cut from the steel plates with the longitudinal axes parallel to the rolling direction. The sample size for tensile testing is based on a laboratory standard, referring to Refs. [39,40]. The tensile specimens were polished to a mirror finish before tensile tests. Quasi-static uniaxial tensile tests were performed in a LTM-20KN testing machine with a strain rate of $3 \times 10^{-3} \text{ s}^{-1}$ at room temperature. The cyclic load-unload-reload (LUR) tensile tests were performed to estimate the Bauschinger effect following the procedure in previous study [39]. During the LUR tensile tests, the specimens were tensioned to an assigned strain, unloaded to 50 N, and then reloaded.

2.3. Microstructural characterization

The cross-section samples were grinded, polished and etched with 2% Nital solution. The microstructures were observed by an optical microscope (OM, Olympus BX41 M) and a scanning electron microscopy (SEM, FEI Quanta 250F). According to the SEM images, volume fraction of martensite was quantitatively analyzed by using Image J software [41]. Electron backscattering diffraction (EBSD) tests were conducted in a Zeiss Auriga focused ion beam/scanning electron microscope to investigate the microstructure of the as-quenched martensite. The scanning step size and accelerating voltage were 500 nm and 15 kV, respectively. X-ray diffractometer (XRD) with Cu K α radiation were performed (scanning from 40° to 100° with the step size of 0.02°) to estimate the dislocation density of the steels according to the literatures [42,43]. The substructures of DP steels were also revealed by a transmission electron microscope (TEM, FEI Tecnai 20) operated at 200 kV. The thin foils for TEM observation were cut parallel to the normal plane and grinded to a thickness of ~60 μm . Finally, the perforation by twin-jet polishing machine was carried out utilizing a solution of 10% perchloric acid and 90% alcohol at -20 °C.

3. Results

3.1. Microstructures

Fig. 2a shows the optical microstructure of the as-received sample which consists of pearlite and ferrite. The volume fraction of ferrite is ~65% with an average grain size of ~25 μm . After quenched from 950 °C, typical lath martensitic structure is obtained, as shown in the inverse pole figure (IPF) in Fig. 2b. The prior austenite grain boundaries (PAGBs) are marked by the white dash lines, indicating an average grain size of ~19.5 μm in as-quenched sample. The austenite grain is divided into the hierarchical structure containing packets, blocks and lath with certain orientation relationships, which are also in line with Ref. [44, 45]. In order to effectively refine the martensitic structure, a novel

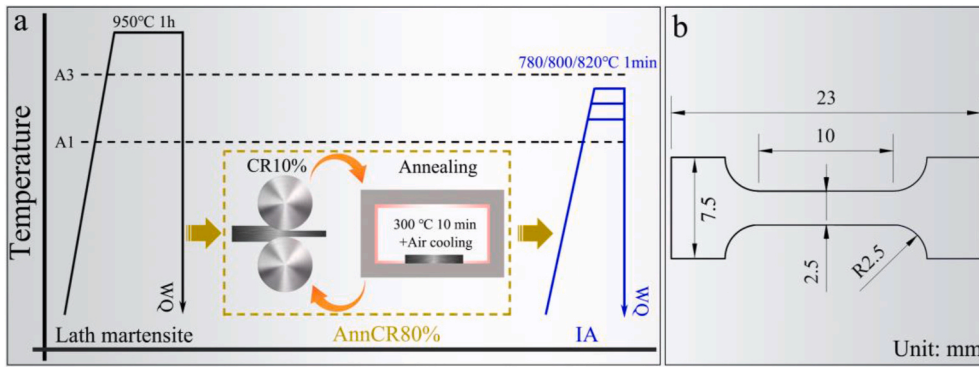


Fig. 1. Illustration of (a) the processing route to preparing UFG-HSDP steels and (b) the dimension of the tensile specimens. A1 and A3 are the starting and finishing temperatures of austenite formation during annealing, respectively; WQ: water quenching; CR: cold-rolling (rolling at room-temperature); AnnCR: cyclic annealing & cold-rolling; IA: intercritical annealing.

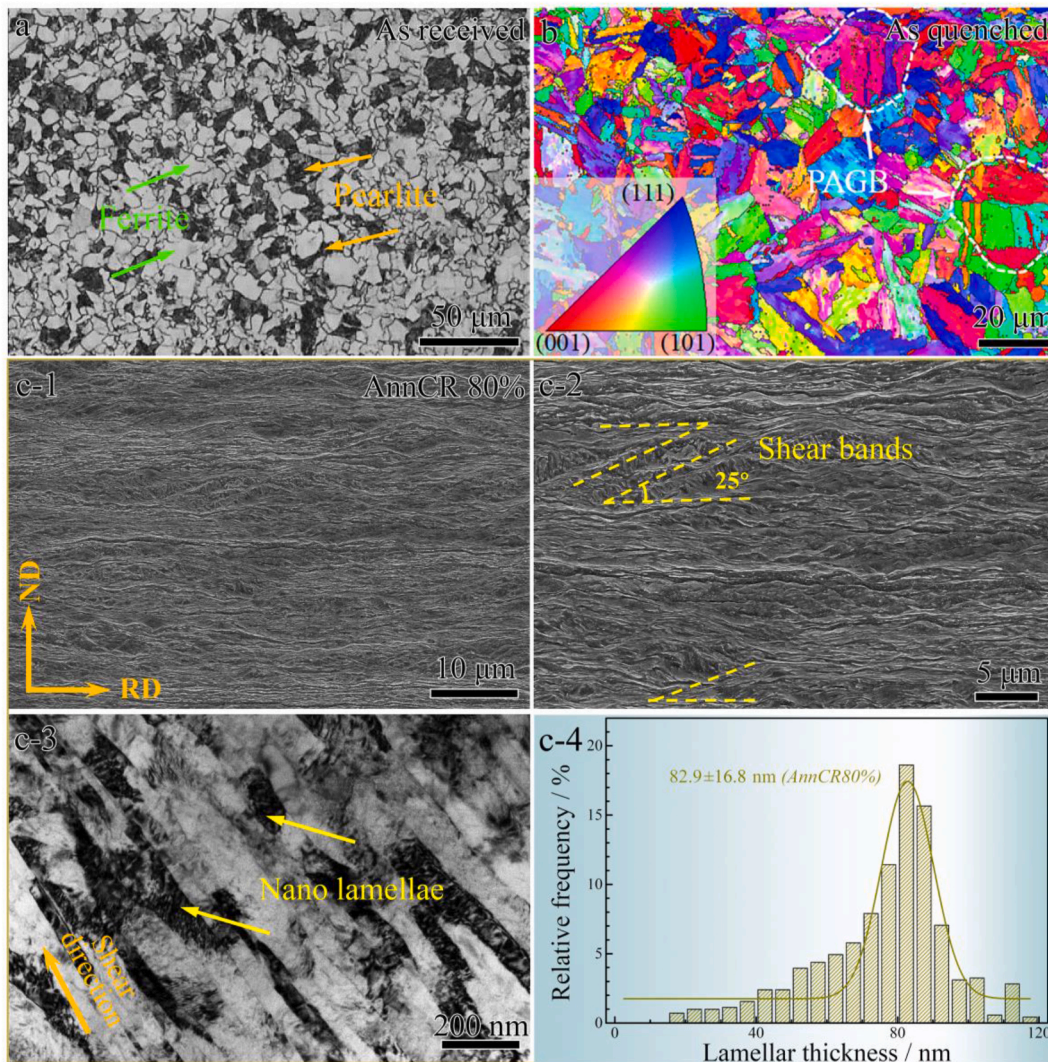


Fig. 2. Microstructure refinement of the low carbon steel by the AnnCR process: (a) optical microstructure of the as-received sample, (b) IPF image of the as-quenched martensitic steel, (c-1) and (c-2) SEM images, (c-3) and (c-4) bright-field TEM image and statistic distribution of lamellar thickness of the 80% rolled sample.

AnnCR processing route was performed on the as-quenched steel. No edge crack occurred in the rolled sheet even the total thickness reduction reached up to 80%. Fig. 2c-1 shows that the microstructure is significantly refined and stretched along the rolling direction (RD) after rolling

reduction of 80%. In some local area, micro-shear bands are formed as shown in Fig. 2c-2, which indicates a strain localization during plastic deformation [46]. Fig. 2c-3 shows the bright-field TEM image of the 80% rolled sample. Lamellar structure parallel to the shear direction is

obtained when the equivalent rolling strain is ~ 1.6 . According to the statistics in Fig. 2c–4, the lamellar thickness ranges from 20 to 120 nm, and the average thickness is ~ 82.9 nm. Therefore, the low carbon steel with nano-lamellar structure is produced by the AnnCR processing at a relatively low equivalent strain.

Fig. 3a–c shows the microstructure of the intercritical annealed samples at 780 °C, 800 °C and 820 °C for 1 min (DP780, DP800 and DP820), respectively. All the microstructures exhibit an equiaxed and uniform distributed UFG ferrite grains with ultra-fine martensite distributed along the grain boundaries. As shown in Fig. 3d, with increasing annealing temperature, the volume fraction of martensite is gradually increased from 39% to 44% and 50%, and the average grain size of ferrite is decreased slightly from 3.2 μm to 2.8 μm and 2.5 μm , respectively. It is suggested that the UFG-DP structure can be produced by intercritical annealing from the nano-lamellar structure with a short annealing time [35].

Fig. 4a shows the bright-field TEM image of DP780 sample. The equiaxed ferritic grains are connected by ferrite grain boundaries (FGBs), marked by the orange dash lines. A small amount of fine martensite islands in size of ~ 200 nm are located at the grain boundary of equiaxed ferrite, forming the ferrite/martensite (F/M) interfaces highlighted by the cyan dash line. Dislocation density in the ferrite grains is very low, which is induced by local deformation for accommodating the martensitic transformation [47,48]. As the annealing temperature is increased to 800 °C (Fig. 4b), more fine martensite islands (~ 1 μm) are formed along the FGBs, resulting in higher fraction of F/M interfaces around the ferrite grain. Meanwhile, high density of dislocations are observed near the F/M interface. Fig. 4c shows an additional growth of martensite surrounding the ferrite grains in the DP820 sample, while the grain size of ferrite is decreased slightly. In this case, the soft ferrite grains are almost roundly constraint by the F/M interfaces, which is the suggested ideal heterostructure to improve the strength and ductility [15,19]. Higher density of dislocations are also

formed in the ferrite grain interior of DP820 sample.

The dislocation density of the three HSDP steels were estimated through the XRD tests according to Refs. [42,43]. Fig. 5a shows the 2 θ -scan profiles of the HSDP steels. As shown in Fig. 5b, the normalized (110) peaks of the samples were extracted from the XRD profiles. It is found that the width of (110) peak in DP820 is broader than that in DP780 and DP800 samples, which indicates higher dislocation density in DP820. The estimated dislocation densities of the DP steels by XRD are $5.8 \times 10^{14} \text{ m}^{-2}$, $5.4 \times 10^{14} \text{ m}^{-2}$, and $6.3 \times 10^{14} \text{ m}^{-2}$, respectively, presenting a similar trend in TEM observation. The higher dislocation density of DP820 is proposed to be induced by the higher volume fraction of martensite [41].

3.2. Mechanical properties

3.2.1. Microhardness of the hetero-zones

Fig. 6a shows the microhardness of the hetero-zones in UFG-HSDP steels. It is clearly that the microhardness of martensite zones is much higher than ferrite zones in the HSDP steels, leading to mechanical incompatibility between the constituent phases. Fig. 6b shows the microhardness evolution of ferrite and martensite zones with martensite volume fraction. The average microhardness of ferrite zones is increased from 175 HV to 276 HV and 292 HV with increasing of martensite content, while the martensite zones show relatively stable microhardness (473 HV, 469HV and 468 HV, respectively). The increase of microhardness of ferrite zones is mainly attributed to the decreased grain size and the increased dislocation density in ferrite as shown in Figs. 3d and 4, respectively.

3.2.2. Tensile property

Fig. 7a shows the engineering stress-strain curves of the steel samples. The as-quenched martensitic steel has a yield strength (YS) and an

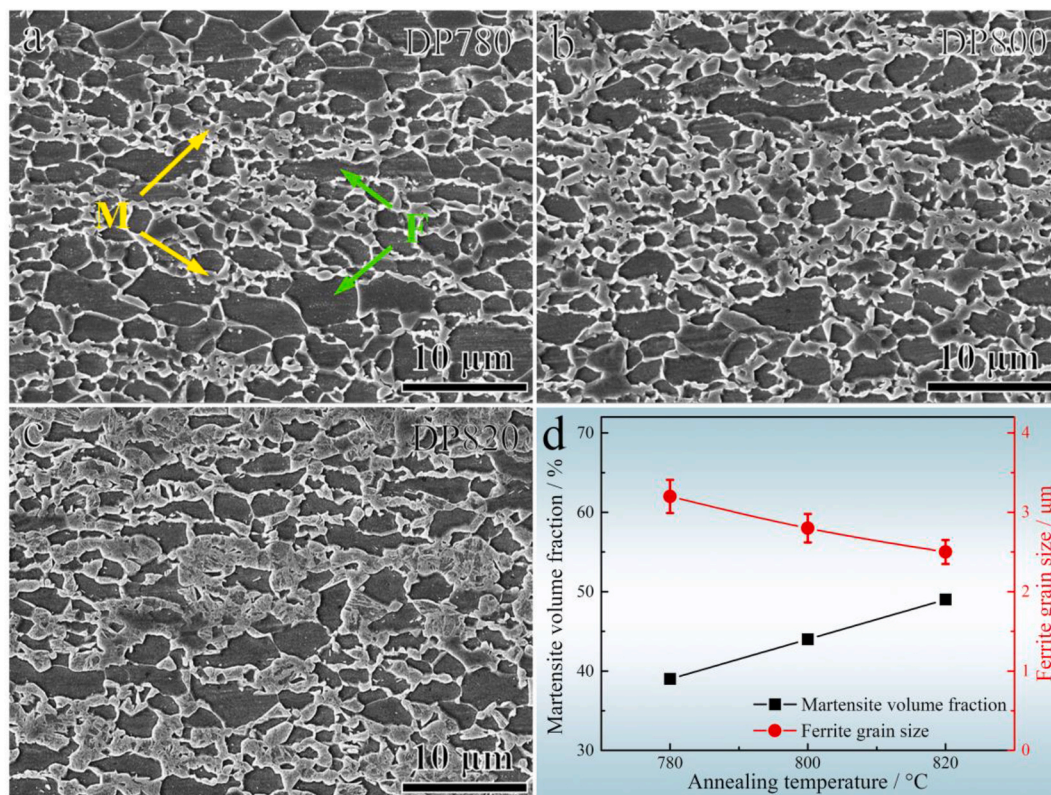


Fig. 3. SEM images of UFG-HSDP steels: (a)–(c) intercritical annealed at 780 °C, 800 °C and 820 °C, respectively, (d) volume fraction of martensite and grain size of ferrite with different annealing temperature.

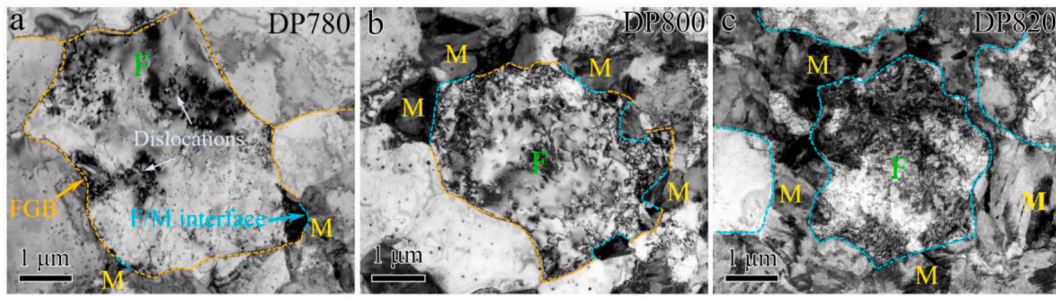


Fig. 4. Bright-field TEM images of UFG-HSDP steels after intercritical annealing: (a) DP780, (b) DP800, and (c) DP820.

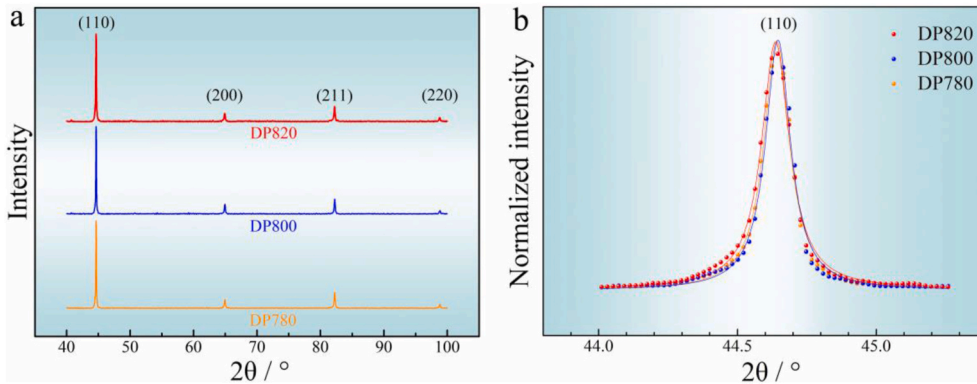


Fig. 5. XRD patterns of the intercritical annealed samples: (a) 2θ-scan profiles and (b) close-up view of normalized (110) peaks.

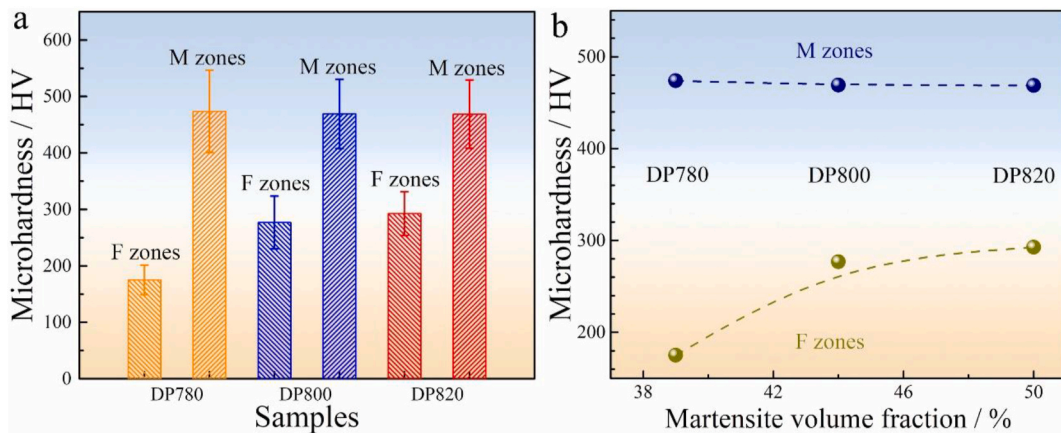


Fig. 6. Microhardness of the hetero-zones in the HSDP steels: (a) microhardness of ferrite and martensite zones of the DP780, DP800 and DP820 samples, (b) evolution of microhardness with martensite volume fractions.

ultimate tensile strength (UTS) of 915 MPa and 1108 MPa, respectively, while the uniform elongation is limited to only 3.8%. After AnnCR processing up to 80% of thickness reduction, the YS of 1761 MPa is notably increased to about twice that of as-quenched martensite and the UTS reaches up to 1823 MPa. The ultra-high strength of the rolled sample is mainly attributed to the extremely refined structure and high density of dislocations [40]. The tensile curves of UFG-HSDP steels obtained by intercritical annealing show typical continuous yield phenomenon. Fig. 7b shows the true stress-strain curves and the corresponding evolution of strain hardening rate (Θ_{Total}) of the as-quenched martensite and UFG-HSDP steels. All steel samples show a high strain hardening rate at the initial stage of deformation, which decreases with straining. The continuous yield and initial high strain hardening rate are mainly resulted from the internal stress introduced by the mechanical incompatibility between the constituent phases and the

unpinned GNDs generated in the ferrite due to martensitic transformation [49]. It is noted that the strain hardening rate of as-quenched martensite declines with strain dramatically, which is resulted from the fine lath structure and high density of dislocations [1]. In comparison, the UFG-HSDP steels show higher level of strain hardening rate than that of as-quenched martensite after strain of 2%, shown in the shadow region of Fig. 7b. The higher strain hardening rate will help with retaining ductility to larger strain according to the Considere criterion for necking in equation (3) [50], where necking will occur when the stress (σ) is larger than the strain hardening rate ($d\sigma/de$).

$$\frac{1}{\sigma} \frac{d\sigma}{de} - 1 \geq 0 \tag{3}$$

As shown in Fig. 7c, with the increase of annealing temperature, the

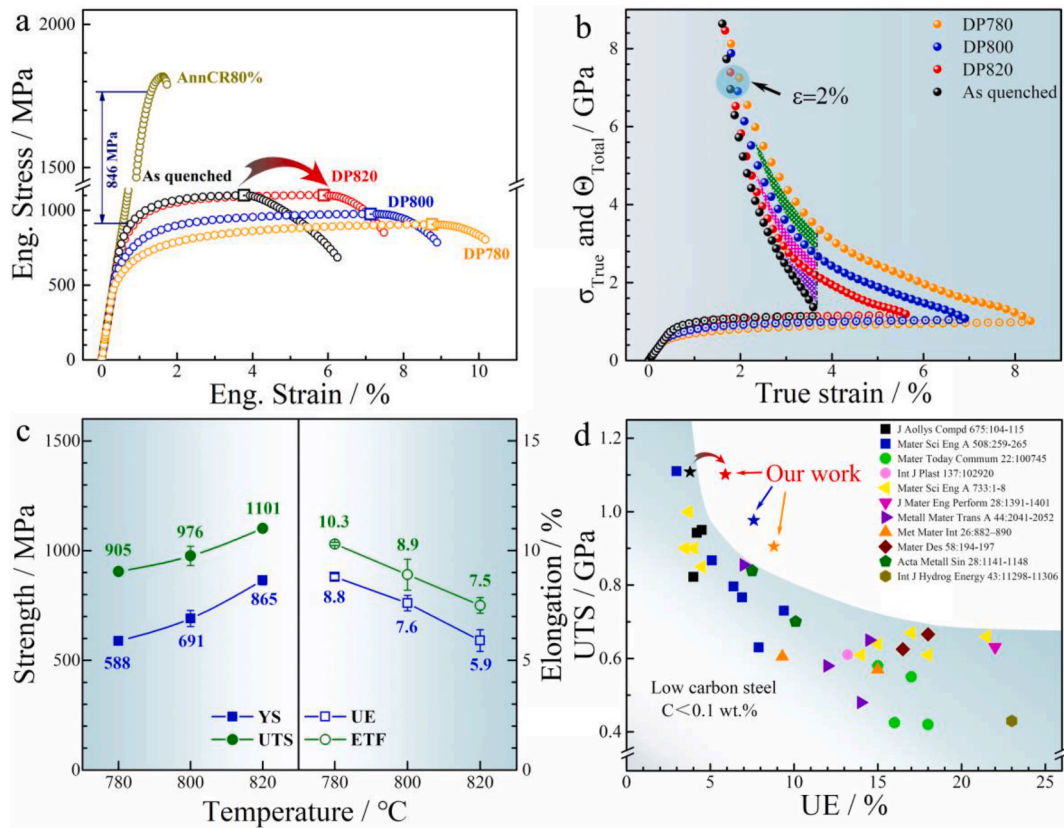


Fig. 7. Mechanical properties of the UFG-HSDP steels: (a) engineering stress-strain curves, (b) true stress-strain and strain hardening rate curves, (c) evolution of YS, UTS, UE and ETF with annealing temperature, (d) mechanical properties of the UFG-HSDP steels compared with the reported data of low-carbon and alloy steels in literatures.

YS of DP steels is increased from 588 MPa to 691 MPa and 865 MPa, and the UTS is increased from 905 MPa to 976 MPa and 1101 MPa, respectively. The uniform elongation (UE) is decreased from 8.8% to 7.6% and 5.9%, and the total elongation to failure (ETF) is decreased from 10.3% to 8.9% and 7.5%, respectively. It is noted that DP820 sample has superior combination of strength and ductility than the as-quenched martensite. The DP820 sample exhibits a much higher ductility than the quenched one with a same strength level. The strategy of obtaining UFG-HSDP structure from the nano-lamellae has been verified to be helpful with improving comprehensive mechanical properties of the low-carbon martensitic steel. As shown in Fig. 7d, the outstanding mechanical properties of UFG-HSDP steels in this work jump out from the region in powder blue, which is plotted by reported data in literatures of low carbon steels with similar compositions.

3.3. Bauschinger effect and HDI hardening

The HDI stress of HSDP steels can be evaluated by the Bauschinger-type cyclic LUR tensile tests, as shown in Fig. 8a. Significant unloading yield drop can be observed from the LUR tensile curves, especially in the 820DP sample, which is mainly related to the mechanical incompatibility between ferrite and martensite. Owing to the huge difference in strength between ferrite and martensite, the soft ferrite begins to deform plastically first, while the hard martensite maintains elastic state. The yield peak occurs due to the load transfer between constituent phases during reloading. Once the martensite yields, rapid relaxation of elastic stresses and strains at F/M interfaces causes the stress drop [38]. The more remarkable yield drop in 820DP sample indicates stronger stress transfer between ferrite and martensite during deformation. The HDI stress can be calculated by the following equations (4) and (5) [15]:

$$\sigma_{\text{HDI}} = \sigma_{\text{flow}} - \sigma_{\text{eff}} \quad (4)$$

$$\sigma_{\text{eff}} = \frac{\sigma_{\text{flow}} - \sigma_u}{2} + \frac{\sigma^*}{2} \quad (5)$$

Where σ_{flow} is the flow stress, σ_{eff} is the effective stress, σ_u is the reverse yield stress and σ^* is called the thermal component of the flow stress or viscous stress, as schematically shown in Fig. 8b.

As shown in Fig. 8c, HDI stress of the samples increases rapidly before strain of 2% and then tend to be stable. In addition, the magnitude of HDI stress in UFG-HSDP steels is increased with the martensite content, which is consistent with the previous studies [38,39]. Fig. 8d-1 shows the HDI hardening curves ($\Theta_{\text{HDI}} = d\sigma_{\text{HDI}}/d\varepsilon$) of three UFG-HSDP steels derived from the HDI stress-strain curves in Fig. 8c. The HDI hardening rate of the three samples are decreased rapidly before strain of 2% then becoming smooth. Fig. 8d-2 shows the variation of the $\Delta\Theta$ between total work hardening rate and HDI hardening rate ($\Delta\Theta = \Theta_{\text{Total}} - \Theta_{\text{HDI}}$) with strain, reflecting the contribution of HDI hardening to the entire work hardening of UFG-HSDP steels during deformation. The $\Delta\Theta$ of UFG-HSDP steels are decreased with strain, suggesting that the HDI hardening capacity enhances with tensile strain, which is probably resulted from the reinforced strain partition and GNDs accumulation during deformation [19,23]. It is shown from the inset of Fig. 8d-2 that when tensile strain is up to 5%, $\Delta\Theta$ of DP820 is close to zero, indicating HDI hardening controls the entire strain hardening rate of the DP820 at higher strain level.

3.4. Fracture analysis

Fig. 9 shows the fracture morphologies of the UFG-HSDP steels. The low-magnitude SEM images show clear necking structure, indicating a

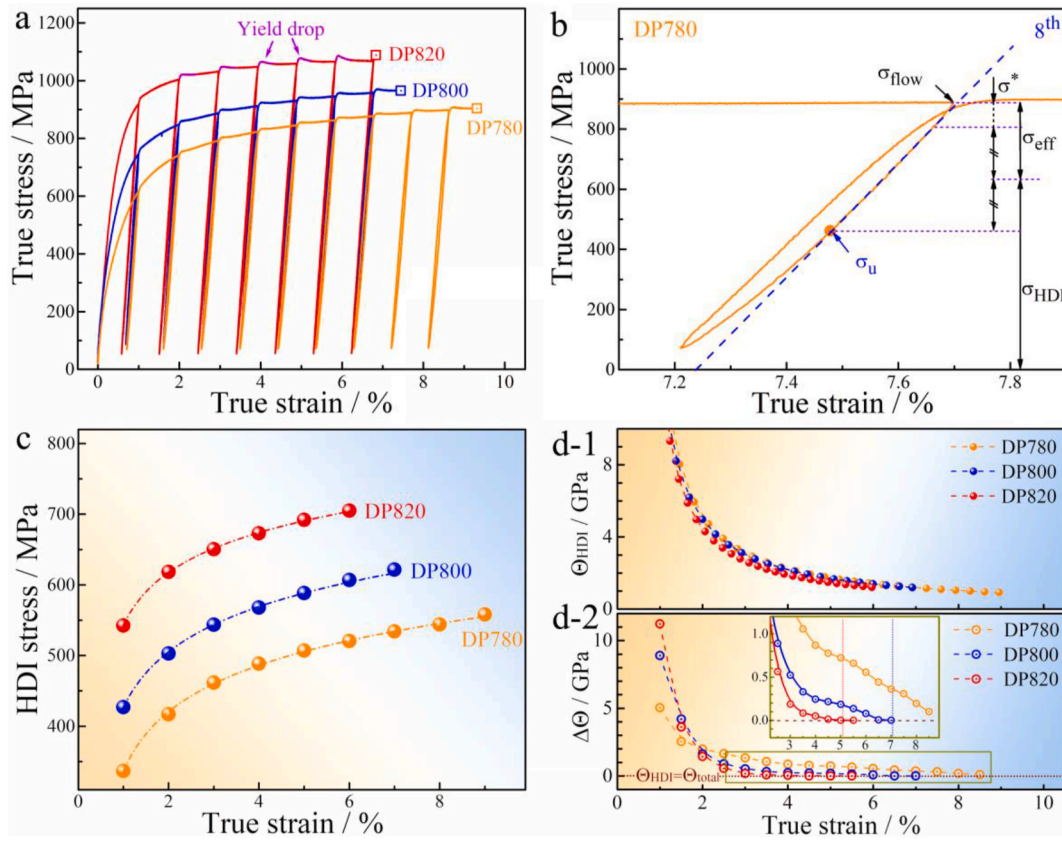


Fig. 8. Bauschinger effect and HDI hardening analysis: (a) LUR true stress-strain curves, (b) schematic of hysteresis loops, (c) evolution of HDI stress with straining, (d-1) and (d-2) evolution of θ_{HDI} and $\Delta\theta$ during tensile deformation.

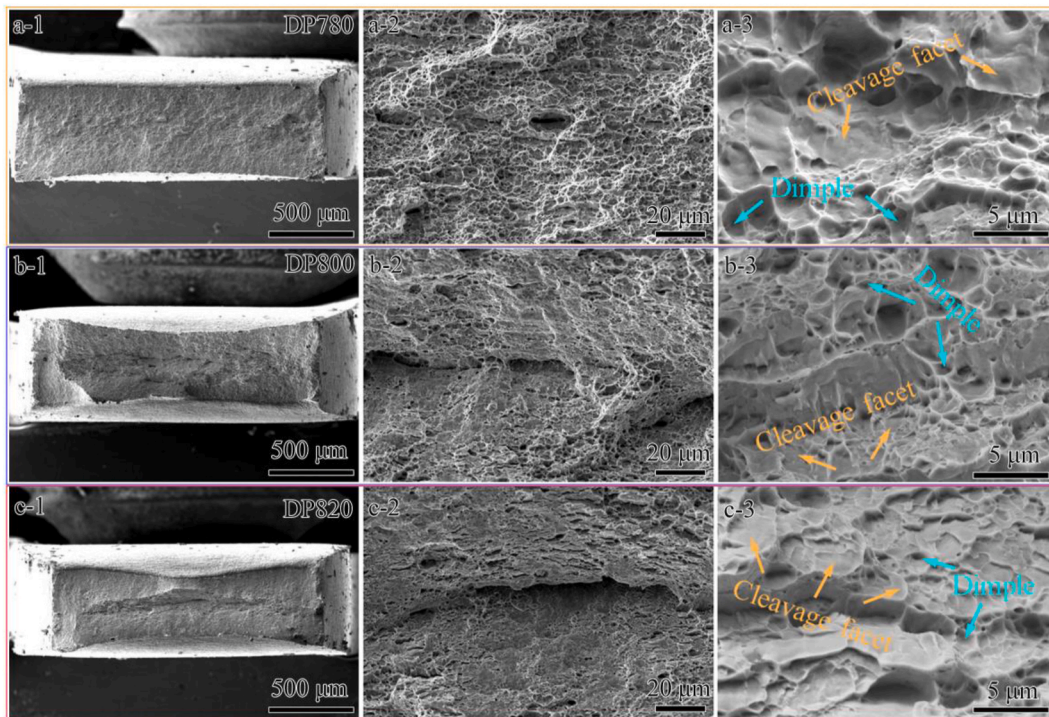


Fig. 9. SEM micrographs of the fracture surfaces of UFG-HSDP steels: (a) DP780, (b) DP800 and (c) DP820.

dominating ductile fracture characteristic of UFG-HSDP steels (Fig. 9a–1 to c-1). It has been reported that ductile fracture of DP steels is usually resulted from a process of nucleation, growth and coalescence of internal voids [51,52]. The high-magnification SEM micrographs in Fig. 9 show that all fracture surfaces of UFG-HSDP steel samples are mixed by cleavage facets and dimples. The observed dimples are small and shallow, especially in the DP820 sample, indicating the limited micro-voids growth. The high density of F/M interfaces in UFG-HSDP steels provide preferential sites for voids nucleation, which inhibits the growth of voids, coalescence of adjacent voids, and results in the fracture surface containing small dimples [53]. The average dimple size of the HSDP steels is decreased from 2.97 μm to 1.69 μm and 1.01 μm , respectively, with increasing martensite volume fraction. The HSDP steels with higher martensite content show increased area fraction of cleavage facets. This brittle fracture feature is mainly resulted from the morphology of interconnected martensite network in UFG-HSDP steels. Firstly, as compared to the isolated martensite islands, the martensite network restrains the plastic deformation of ferrite by confining the slip systems and results in the high level of stress triaxiality [54]. Secondly, damage in the UFG-HSDP steels is preferentially nucleated in the martensite with limited ductility and high stress concentration. Thirdly, the release of stored elastic energy during deformation will result in the unstable crack growth once the crack occurs. As a result, once the martensite fracture is nucleated, the abovementioned stress triaxiality, stress concentration, and rapid release of elastic energy contribute to the cleavage cracking in the ferrite adjacent to damaged martensite.

4. Discussion

4.1. Formation of the nano-lamellar structure and UFG-HSDP steels

As is revealed in Fig. 2, low carbon steels with nano-lamellar structure are produced by the novel AnnCR processing route. The average lamellar thickness of the processed steels is effectively refined to 82.9 nm with a low equivalent strain of ~ 1.6 . Thus, the efficiency of grain refinement using AnnCR processing route is much higher than that of by conventional cold rolling [55]. It is found that the refinement of martensitic structure is mainly related to the motion of solute C atoms occurred during cyclic AnnCR. In order to clarify the in-depth mechanism, the 40% cold-rolled martensitic steels were annealed at different temperatures (from 100 $^{\circ}\text{C}$ to 400 $^{\circ}\text{C}$). As shown in Fig. 10a, annealing induced hardening is found in all the heat-treated samples at 100 $^{\circ}\text{C}$ to 300 $^{\circ}\text{C}$ by testing their microhardness. The peak hardness is obtained in the sample annealed at 300 $^{\circ}\text{C}$ for 10 min. This annealing-induced hardening phenomenon has also been reported in the nanostructured steels processed by severe plastic deformation [56,57], which is

attributed to the interactions between interstitial carbon and defects. As illustrated in Fig. 10b, the martensitic transformation and cold rolling induce high density of dislocations to the quenched martensite in present work. The carbon atoms are segregated to the dislocation cores by subsequent annealing, and produces a pinning effect on dislocation slipping [40,58]. In the next pass of rolling, the interaction between C atoms and dislocations inhibits dynamic recovery and hinders dislocation motion, thus accumulating dislocations significantly. Therefore, deformation-induced refinement is enhanced due to the boosted dislocation generations and impeded dynamic recovery. Additionally, owing to the blocking effect on dislocation slips, the micro shear bands form in the 80% rolled sample, becoming an alternative mechanism to accommodate plastic deformation and refine the microstructures [59].

Within only 1 min, the equiaxed ferrite as well as the high volume fraction of martensite formed rapidly, due to the high driving force of austenite formation and ferrite recrystallization, induced by the nano-lamellar structure. Previous studies reported that the formation and distribution of austenite are significantly influenced by the initial microstructure, which controls the competition between the recrystallization and the austenite formation during annealing [60,61]. Tokizane [62] found that the nucleation of austenite happened simultaneously with the recrystallization, if the initial microstructure was a heavily deformed lath martensite. They also found the enhanced kinetics for austenite formation could result in a high-density fine-grained austenite dispersed in microstructure. In present study, the nano-lamellar structure introduces high density dislocations and interfaces, providing numerous nucleation sites for austenite formation. Due to the accelerated austenite formation, higher volume fraction of refined martensite form during the short-time annealing. In addition, the austenite nearby the ferrite grain boundaries impedes the migration of the interface and restrains the growth of recrystallized ferrite grains [63]. Consequently, the ultra-fine DP structure can be maintained at high annealing temperatures. Note that, the ferrite grains are in equiaxed shape, indicating that recrystallization of ferrite is not suppressed completely, due to the large driving force of nano-lamellae microstructure.

4.2. Strengthening mechanism of the UFG-HSDP steels

The UFG-HSDP steels derived from the nano-lamellae structure exhibit an outstanding mechanical property, as shown in Fig. 7d. Especially, the DP820 sample has a much higher ductility than the as-quenched martensite, while they have an almost same strength level. The superior mechanical property of UFG-HSDP steel is mainly due to the significant grain refinement, as well as the architecture of dual-phase heterostructure. On one hand, the UFG in HSDP steels is undoubtedly

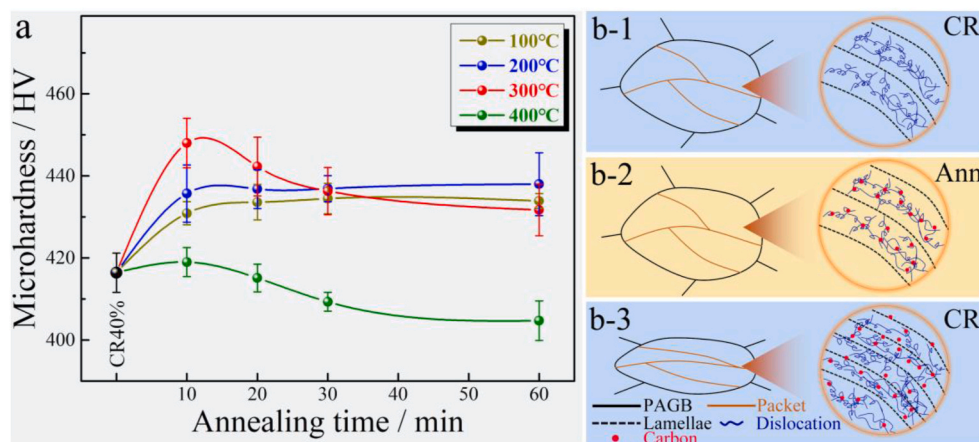


Fig. 10. Microstructural responses of the martensite during AnnCR. (a) microhardness of the 40% rolled martensite annealed at different temperatures, (b-1)–(b-3) schematic illustration of the interactions between C atoms and dislocations during AnnCR.

resulted from the initial nano lamellar structure, although the speed of recovery and recrystallization is high during the short-time annealing. With increasing martensite volume fraction, the yield strength is improved in the DP820 sample, in conjunction with the decreased ferrite grain size and the increased dislocation density. On the other hand, the mechanical incompatibility between ferrite and martensite results in significant stress/strain partition between constituent phases. Consequently, strain gradient and GNDs piling-up occur nearby the F/M interfaces, which produces back stress and forward stress in soft ferrite and hard martensite, respectively. The back stress and forward stress collectively produce the HDI stress [19]. As indicated by Fig. 6c and d, HDI stress increases with the applied strain, resulting in an extra work hardening to the DP steels. It is found that HDI strengthening is influenced by the content and morphology of martensite. The DP820 sample where equiaxed ferrite are completely surrounded by martensite shows higher HDI stress and stronger HDI hardening, especially at high tensile strain. The high HDI stress in DP820 sample leads to a significant enhancement of yield strength [64,65]. In addition, the strong HDI hardening helps with enhancing the strain hardening rate to maintain a good ductility. The main factors to influence the HDI hardening in DP820 are listed as follows: First, higher martensite volume fraction in DP820 produces a high density of zone interfaces, which promotes the strain partitioning and GND accumulations [19]. Second, the embedded equiaxed ferrite grains with several micrometers have enough space for the piling-up of GNDs. Thus, the DP820 sample meets the design criteria for maximizing HDI hardening in HSMS [20]. Therefore, the DP820 sample has a close high strength to the as-quenched sample, while the ductility is improved significantly.

5. Conclusion

UFG-HSDP steels were prepared by cyclic annealing & cold-rolling and subsequent intercritical annealing, which produced superior combination of strength and ductility. The microstructure, mechanical properties and fracture behavior of UFG-HSDP steels were studied systematically. The effects of HDI stress/hardening on mechanical properties of UFG-HSDP steels were analyzed by LUR tensile tests. The key conclusions are as follows:

- 1 A nano-lamellar low carbon steel with spacing of 82.9 nm was produced from a martensitic structure by the AnnCR under a thickness reduction of 80%. The efficient grain refinement is mainly resulted from the interaction between carbon atoms and dislocations at 300 °C. The annealing promotes carbon atoms moving to the dislocation core and produces a pinning effect, which inhibits dynamic recovery and boosts dislocation generation in the subsequent rolling, thus refining the microstructure effectively.
2. After intercritical annealing, the HSDP structure composed of fine equiaxed ferrite and martensite was obtained. The volume fraction of martensite ranges from 39% to 50% and the average ferrite grain size is about 3 μm. The DP820 sample with highest martensite content shows an ideal hetero-structured morphology, in which the equiaxed ferrite grains are constrained by the surrounding hard martensite.
3. Increasing volume fraction of martensite results in the enhanced YS, UTS and decreased UE of UFG-HSDP steels. Compared with the as-quenched martensite sample, the DP820 sample exhibits a same high strength level (YS: 865 MPa; UTS: 1101 MPa), but the UE is increased to 6%. The superior tensile property of the UFG-HSDP steels is attributed to the higher strain hardening capacity than as-quenched martensite.
4. As the martensite content is increased, a higher Bauschinger effect and a higher HDI stress are tested in the UFG-HSDP steels. The proposed microstructure of DP820 where the equiaxed ferrite grains are constraint effectively by the surrounding martensite helps with the improving HDI stress and hardening. The extraordinary HDI strengthening enhances strength and sustains ductility of HSDP steels simultaneously.
5. The ductile fracture of UFG-HSDP steels is characteristic as a mixed dimples and cleavage facets. The micro-voids are generally small and shallow. As the volume fraction of martensite is increased, the number of cleavage facets is increased.

Declaration of competing interest

The authors declare that they have no known competing financial interests or personal relationships that could have appeared to influence the work reported in this paper.

Acknowledgement

This work was supported by the Key Program of National Natural Science Foundation of China (grant number 51931003), the National Natural Science Foundation of China (grant numbers 52071178, 51901103), the Hong Kong Research Grants Council (GRF 11214121), the Projects in Science and Technique Plans of Ningbo City (grant number 2019B10083), the China Post-doctoral Science Foundation (grant number 2021M701715) and the Fundamental Research Funds for the Central Universities (grant number 30918011342). We also thank the technical support from the Jiangsu Key Laboratory of Advanced Micro&Nano Materials and Technology. The SEM and TEM experiments are performed at the Materials Characterization and Research Center of Nanjing University of Science and Technology.

References

- [1] M. Michiuchi, S. Nambu, Y. Ishimoto, J. Inoue, T. Koseki, Relationship between local deformation behavior and crystallographic features of as-quenched lath martensite during uniaxial tensile deformation, *Acta Mater.* 57 (18) (2009) 5283–5291.
- [2] J.M. Park, D.C. Yang, H.-J. Kim, D.G. Kim, S. Lee, H.S. Kim, S.S. Sohn, Ultra-strong and strain-hardenable ultrafine-grained medium-entropy alloy via enhanced grain-boundary strengthening, *Mater. Res. Lett.* 9 (7) (2021) 315–321.
- [3] H. Li, S. Gao, Y. Tomota, I. Seiichiro, N. Tsuji, T. Ohmura, Mechanical response of dislocation interaction with grain boundary in ultrafine-grained interstitial-free steel, *Acta Mater.* 206 (2021) 116621.
- [4] L.R.C. Malheiros, E.A.P. Rodriguez, A. Arlazarov, Mechanical behavior of tempered martensite: Characterization and modeling, *Mater. Sci. Eng., A* 706 (2017) 38–47.
- [5] J. Li, B. Gao, Z. Huang, H. Zhou, Q. Mao, Y. Li, Design for strength-ductility synergy of 316L stainless steel with heterogeneous lamella structure through medium cold rolling and annealing, *Vacuum* 157 (2018) 128–135.
- [6] S. Ghosh, S. Mula, Improvement of fracture toughness of Ti+Nb stabilized microalloyed and interstitial free steels processed through single phase regime control multiaxial forging, *Mater. Sci. Eng., A* 772 (2020) 138817.
- [7] S. Ghosh, J. Kömi, S. Mula, Flow stress characteristics and design of innovative 3-steps multiphase control thermomechanical processing to produce ultrafine grained bulk steels, *Mater. Des.* 186 (2020) 108297.
- [8] S. Ghosh, N. Bibhanshu, S. Suwas, K. Chatterjee, Surface mechanical attrition treatment of additively manufactured 316L stainless steel yields gradient nanostructure with superior strength and ductility, *Mater. Sci. Eng., A* 820 (2021) 141540.
- [9] S. Ghosh, S. Mula, Fracture toughness characteristics of ultrafine grained Nb–Ti stabilized microalloyed and interstitial free steels processed by advanced multiphase control rolling, *Mater. Char.* 159 (2020) 110003.
- [10] A. Järvenpää, S. Ghosh, A. Khosravifard, M. Jaskari, A. Hamada, A new processing route to develop nano-grained structure of a TRIP-aided austenitic stainless-steel using double reversion fast-heating annealing, *Mater. Sci. Eng. A* 808 (2021) 140917.
- [11] S. Ghosh, S. Mula, D. Kumar Mondal, Development of ultrahigh strength cast-grade microalloyed steel by simple innovative heat treatment techniques for industrial applications, *Mater. Sci. Eng., A* 700 (2017) 667–680.
- [12] I. Miettunen, S. Ghosh, M.C. Somani, S. Pallaspuuro, J. Kömi, Competitive mechanisms occurring during quenching and partitioning of three silicon variants of 0.4 wt.% carbon steels, *J. Mater. Res. Technol.* 11 (2021) 1045–1060.
- [13] S. Ghosh, I. Miettunen, M.C. Somani, J. Kömi, D. Porter, Nanolath martensite-austenite structures engineered through DQ&P processing for developing tough, ultrahigh strength steels, *Mater. Today Proc.* 46 (2021) 2131–2134.
- [14] I.H. Miettunen, S. Ghosh, M.C. Somani, S. Pallaspuuro, D. Porter, J. Kömi, Effect of silicon content on the decomposition of austenite in 0.4C steel during quenching and partitioning treatment, *Mater. Sci. Forum* 1016 (2021) 1361–1367.
- [15] X. Wu, M. Yang, F. Yuan, G. Wu, Y. Wei, X. Huang, Y. Zhu, Heterogeneous lamella structure unites ultrafine-grain strength with coarse-grain ductility, *Proc. Natl. Acad. Sci. U.S.A.* 112 (47) (2015) 14501–14505.

- [16] C. Huang, Y. Wang, X. Ma, S. Yin, H. Höppel, M. Göken, X. Wu, H. Gao, Y. Zhu, Interface affected zone for optimal strength and ductility in heterogeneous laminate, *Mater. Today* 21 (7) (2018) 713–719.
- [17] C. Tan, Y. Chew, R. Duan, F. Weng, S. Sui, F.L. Ng, Z. Du, G. Bi, Additive manufacturing of multi-scale heterostructured high-strength steels, *Mater. Res. Lett.* 9 (7) (2021) 291–299.
- [18] J. Li, S. Wang, Q. Mao, Z. Huang, Y. Li, Soft/hard copper/bronze laminates with superior mechanical properties, *Mate. Sci. Eng. A* 756 (2019) 213–218.
- [19] Y. Zhu, K. Ameyama, P.M. Anderson, I.J. Beyerlein, H. Gao, H.S. Kim, E. Lavernia, S. Mathaudhu, H. Mughrabi, R.O. Ritchie, Heterostructured materials: superior properties from hetero-zone interaction, *Mater. Res. Lett.* 9 (1) (2021) 1–31.
- [20] X. Wu, Y. Zhu, Heterogeneous materials: a new class of materials with unprecedented mechanical properties, *Mater. Res. Lett.* 5 (8) (2017) 527–532.
- [21] Y.F. Wang, M.S. Wang, X.T. Fang, F.J. Guo, H.Q. Liu, R.O. Scattergood, C.X. Huang, Y.T. Zhu, Extra strengthening in a coarse/ultrafine grained laminate: role of gradient interfaces, *Int. J. Plast.* 123 (2019) 196–207.
- [22] Y. Wang, Y. Wei, Z. Zhao, Z. Lin, F. Guo, Q. Cheng, C. Huang, Y. Zhu, Mechanical response of the constrained nanostructured layer in heterogeneous laminate, *Scripta Mater.* 207 (2022) 114310.
- [23] Y. Zhu, X. Wu, Perspective on hetero-deformation induced (HDI) hardening and back stress, *Mater. Res. Lett.* 7 (10) (2019) 393–398.
- [24] J. Li, M. Zhao, L. Jin, F. Wang, S. Dong, J. Dong, Simultaneously improving strength and ductility through laminate structure design in Mg–8.0Gd–3.0Y–0.5Zr alloys, *J. Mater. Sci. Technol.* 71 (2021) 195–200.
- [25] X. Li, L. Lu, J. Li, X. Zhang, H. Gao, Mechanical properties and deformation mechanisms of gradient nanostructured metals and alloys, *Nat. Rev. Mater.* 5 (9) (2020) 706–723.
- [26] K. Lu, Making strong nanomaterials ductile with gradients, *Science* 345 (6203) (2014) 1455.
- [27] R. Geng, Q. Zhao, F. Qiu, Q. Jiang, Simultaneously increased strength and ductility via the hierarchically heterogeneous structure of Al-Mg-Si alloys/nanocomposite, *Mater. Res. Lett.* 8 (6) (2020) 225–231.
- [28] T.Q. Mo, Z.J. Chen, H. Chen, C. Hu, W.J. He, Q. Liu, Multiscale interfacial structure strengthening effect in Al alloy laminated metal composites fabricated by accumulative roll bonding, *Mater. Sci. Eng., A* 766 (2019) 138354.
- [29] C. Zhang, C. Zhu, P. Cao, X. Wang, F. Ye, K. Kaufmann, L. Casalena, B. E. MacDonald, X. Pan, K. Vecchio, E.J. Lavernia, Aged metastable high-entropy alloys with heterogeneous lamella structure for superior strength-ductility synergy, *Acta Mater.* 199 (2020) 602–612.
- [30] C. Sawangrat, S. Kato, D. Orlov, K. Ameyama, Harmonic-structured copper: performance and proof of fabrication concept based on severe plastic deformation of powders, *J. Mater. Sci.* 49 (19) (2014) 6579–6585.
- [31] P. Peng, A. Tang, J. She, J. Zhang, S. Zhou, K. Song, F. Pan, Significant improvement in yield stress of Mg-Gd-Mn alloy by forming bimodal grain structure, *Mater. Sci. Eng., A* 803 (2021) 140569.
- [32] A.-P. Pierman, O. Bouaziz, T. Pardoen, P. Jacques, L. Brassart, The influence of microstructure and composition on the plastic behaviour of dual-phase steels, *Acta Mater.* 73 (2014) 298–311.
- [33] M. Balbi, I. Alvarez-Armas, A. Armas, Effect of holding time at an intercritical temperature on the microstructure and tensile properties of a ferrite-martensite dual phase steel, *Mater. Sci. Eng., A* 733 (2018) 1–8.
- [34] H. Mirzadeh, M. Alibeyki, M. Najafi, Unraveling the initial microstructure effects on mechanical properties and work-hardening capacity of dual-phase steel, *Metal. Mater. Trans. A* 48 (10) (2017) 4565–4573.
- [35] A.G. Kalashami, A. Keranpur, A. Najafzadeh, Y. Mazaheri, Development of a high strength and ductile Nb-bearing dual phase steel by cold-rolling and intercritical annealing of the ferrite-martensite microstructures, *Mater. Sci. Eng., A* 658 (2016) 355–366.
- [36] M. Alibeyki, H. Mirzadeh, M. Najafi, Fine-grained dual phase steel via intercritical annealing of cold-rolled martensite, *Vacuum* 155 (2018) 147–152.
- [37] S. Etesami, M. Enayati, A.G. Kalashami, Austenite formation and mechanical properties of a cold rolled ferrite-martensite structure during intercritical annealing, *Mater. Sci. Eng., A* 682 (2017) 296–303.
- [38] B. Gao, X. Chen, Z. Pan, J. Li, Y. Ma, Y. Cao, M. Liu, Q. Lai, L. Xiao, H. Zhou, A high-strength heterogeneous structural dual-phase steel, *J. Mater. Sci.* 54 (19) (2019) 12898–12910.
- [39] B. Gao, R. Hu, Z. Pan, X. Chen, Y. Liu, L. Xiao, Y. Cao, Y. Li, Q. Lai, H. Zhou, Strengthening and ductilization of laminate dual-phase steels with high martensite content, *J. Mater. Sci. Technol.* 65 (2021) 29–37.
- [40] B. Gao, Q. Lai, Y. Cao, R. Hu, L. Xiao, Z. Pan, N. Liang, Y. Li, G. Sha, M. Liu, H. Zhou, X. Wu, Y. Zhu, Ultrastrong low-carbon nanosteel produced by heterostructure and interstitial mediated warm rolling, *Sci. Adv.* 6 (39) (2020), eaba8169.
- [41] Q. Lai, L. Brassart, O. Bouaziz, M. Gouné, M. Verdier, G. Parry, A. Perlade, Y. Bréchet, T. Pardoen, Influence of martensite volume fraction and hardness on the plastic behavior of dual-phase steels: experiments and micromechanical modeling, *Int. J. Plast.* 80 (2016) 187–203.
- [42] L.R. Xiao, Y. Cao, S. Li, H. Zhou, X.L. Ma, L. Mao, X.C. Sha, Q.D. Wang, Y.T. Zhu, X. D. Han, The formation mechanism of a novel interfacial phase with high thermal stability in a Mg-Gd-Y-Ag-Zr alloy, *Acta Mater.* 162 (2019) 214–225.
- [43] Y. Liu, Y. Cao, Q. Mao, H. Zhou, Y. Zhao, W. Jiang, Y. Liu, J.T. Wang, Z. You, Y. Zhu, Critical microstructures and defects in heterostructured materials and their effects on mechanical properties, *Acta Mater.* 189 (2020) 129–144.
- [44] C. Du, J.P.M. Hoefnagels, R. Vaes, M.G.D. Geers, Block and sub-block boundary strengthening in lath martensite, *Scripta Mater.* 116 (2016) 117–121.
- [45] L. Morsdorf, O. Jeannin, D. Barbier, M. Mitsuhashi, D. Raabe, C.C. Tasan, Multiple mechanisms of lath martensite plasticity, *Acta Mater.* 121 (2016) 202–214.
- [46] A.A. Tiarniyu, A.G. Odeshi, J.A. Szpunar, Multiple strengthening sources and adiabatic shear banding during high strain-rate deformation of AISI 321 austenitic steel: effects of grain size and strain rate, *Mater. Sci. Eng., A* 711 (2018) 233–249.
- [47] C. Tian, D. Ponge, L. Christiansen, C. Kirchlechner, On the mechanical heterogeneity in dual phase steel grades: activation of slip systems and deformation of martensite in DP800, *Acta Mater.* 183 (2020) 274–284.
- [48] A. Kundu, D.P. Field, Influence of plastic deformation heterogeneity on development of geometrically necessary dislocation density in dual phase steel, *Mater. Sci. Eng., A* 667 (2016) 435–443.
- [49] M. Calcagnotto, Y. Adachi, D. Ponge, D. Raabe, Deformation and fracture mechanisms in fine and ultrafine-grained ferrite/martensite dual-phase steels and the effect of aging, *Acta Mater.* 59 (2) (2011) 658–670.
- [50] Y.T. Zhu, X.L. Wu, Ductility and plasticity of nanostructured metals: differences and issues, *Mater. Today Nano* 2 (2018) 15–20.
- [51] Y. Liu, D. Fan, S.P. Bhat, A. Srivastava, Ductile fracture of dual-phase steel sheets under bending, *Int. J. Plast.* 125 (2020) 80–96.
- [52] J. Kaddhodapour, A. Butz, S.Z. Rad, Mechanisms of void formation during tensile testing in a commercial, dual-phase steel, *Acta Mater.* 59 (7) (2011) 2575–2588.
- [53] N. Saeidi, F. Ashrafzadeh, B. Niroumand, Development of a new ultrafine grained dual phase steel and examination of the effect of grain size on tensile deformation behavior, *Mater. Sci. Eng., A* 599 (2014) 145–149.
- [54] Q. Lai, O. Bouaziz, M. Gouné, L. Brassart, M. Verdier, G. Parry, A. Perlade, Y. Bréchet, T. Pardoen, Damage and fracture of dual-phase steels: influence of martensite volume fraction, *Mater. Sci. Eng., A* 646 (2015) 322–331.
- [55] X. Huang, S. Morito, N. Hansen, T. Maki, Ultrafine structure and high strength in cold-rolled martensite, *Metal. Mater. Trans. A* 43 (10) (2012) 3517–3531.
- [56] L.X. Sun, N.R. Tao, M. Kuntz, J.Q. Yu, K. Lu, Annealing-induced hardening in a nanostructured low-carbon steel prepared by using dynamic plastic deformation, *J. Mater. Sci. Technol.* 30 (8) (2014) 731–735.
- [57] J.G. Kim, J.B. Seol, J.W. Bae, H.S. Kim, On the mechanistic understanding of annealing-induced strength enhancement of ultrafine-grained high-Mn steel, *Materialia* 13 (2020) 100837.
- [58] L. Zhou, F. Fang, X. Zhou, Y. Tu, Z. Xie, J. Jiang, Cementite nano-crystallization in cold drawn pearlitic wires instigated by low temperature annealing, *Scripta Mater.* 120 (2016) 5–8.
- [59] P. Hua, K. Chu, Q. Sun, Grain refinement and amorphization in nanocrystalline NiTi micropillars under uniaxial compression, *Scripta Mater.* 154 (2018) 123–126.
- [60] C. Zheng, D. Raabe, Interaction between recrystallization and phase transformation during intercritical annealing in a cold-rolled dual-phase steel: a cellular automaton model, *Acta Mater.* 61 (14) (2013) 5504–5517.
- [61] S.A. Etesami, M.H. Enayati, A.G. Kalashami, Austenite formation and mechanical properties of a cold rolled ferrite-martensite structure during intercritical annealing, *Mater. Sci. Eng., A* 682 (2017) 296–303.
- [62] M. Tokizane, N. Matsumura, K. Tsuzaki, T. Maki, I. Tamura, Recrystallization and formation of austenite in deformed lath martensitic structure of low carbon steels, *Metal. Trans. A* 13 (8) (1982) 1379–1388.
- [63] Pan B. Gao, Q. Lai, X. Chen, Y. Cao, M. Liu, H. Zhou, Microstructure and mechanical properties of a cold-rolled ultrafine-grained dual-phase steel, *Materials* 11 (8) (2018) 1399.
- [64] D. Kong, C. Dong, X. Ni, Z. Liang, C. Man, X. Li, Hetero-deformation-induced stress in additively manufactured 316L stainless steel, *Mater. Res. Lett.* 8 (10) (2020) 390–397.
- [65] J. Moon, J.M. Park, J.W. Bae, N. Kang, J. Oh, H. Shin, H.S. Kim, Hetero-deformation-induced strengthening by twin-mediated martensitic transformation in an immiscible medium-entropy alloy, *Scripta Mater.* 186 (2020) 24–28.